Semnan University

Progress in Physics of Applied Materials

journal homepage: https://ppam.semnan.ac.ir/

Numerical study of frequency effect on induction heating process in three dimensional

Abdol Jabbar Shokri *

Department of Science, Payame Noor University, Tehran, Iran

ARTICLE INFO

Article history:
Received: 14 January 2024
Revised: 16 February 2024
Accepted: 28 February 2024

Keywords:
Frequency
Simulation
Induction heating
Finite element method

ABSTRACT

In this article, we investigate the effect of frequency as one of the important factors in the three-dimensional process of induction heating through numerical modelling. Induction heating is the process of heating electrically conductive materials by electromagnetic induction, which induces an eddy current within the material. Using the finite element method (FEM) and the comsol multiphysics software, we calculate the eddy current and the distribution of heat generated in both the workpiece and the inductor for different frequencies within the range of 0.75-5 kHz. To accomplish this, we utilize a real coil with a helix shape and a cylindrical workpiece. The results demonstrate that as the frequency increases, both the eddy current and the generated heat are transferred to the outer surface of the workpiece, becoming concentrated in a thin layer. In other words, these parameters exponentially decrease along the radius of the workpiece from the surface towards its interior.

1. Introduction

In recent decades, induction heating has emerged as a popular technique in thermal operations involving metals, such as hardening, soldering, brazing, crystal growth, and more. It has been widely applied [1-5]. Apart from its applications in metallurgical industries, induction heat processes are also employed in medical contexts, such as hyperthermia treatment. When compared to other methods like resistance heating and fossil fuels, induction heating offers the following advantages: a) being fast, b) applicable in vacuum, c) easy to control, d) being clean, e) using renewable energies as its source and f) high efficient. One common induction heating system has three major parts: 1) electrical power source, 2) coil (inductor) and 3) workpiece, Fig.1[6,7]. The energy transfer mechanism in this method occurs via electromagnetic fields. In this process, an AC source is connected to the coil to generate time-variable electromagnetic fields. These electromagnetic fields lead to production eddy currents with same as frequency as the applied source but in the opposite direction toward the coil's current in the workpiece and other metallic parts of system near the coil. Due to Joule effect (I^2R), the eddy currents produce heat in metallic parts [4, 8].

Induction heating is a complex process due to its nature as a multiphysical phenomenon. It involves the intricate interaction of electromagnetic phenomena, heat transfer, and metallurgical phenomena. These factors are highly interconnected and nonlinear. Consequently, designing induction-based systems using a trial-and-error method is not only costly but also time-consuming in practice. Therefore, the utilization of computer modeling as a powerful tool can provide a clear understanding of induction heating. In other words, computer simulations offer valuable opportunities to obtain information about quantities that play a crucial role in the induction heating process. So far, computer modeling has been employed to study various parameters such as coil geometry and position effects [9], workpiece geometry (particularly in the field of crystal growth) [10], and input current form [11]. However, these studies have primarily been conducted in 2D. One critical factor that significantly influences the establishment of induction heating is the selection of frequency [12]. The frequency of the current source directly

* Corresponding author.
E-mail address: ajshokri1975@pnu.ac.ir

Cite this article as:
Shokri, A.J., 2024. Numerical study of frequency effect on induction heating process in three dimensional. *Progress in Physics of Applied Materials*, 4(1), pp.21-26.DOI: **10.22075/PPAM.2024.32977.1083**

affects the heat rate and pattern generated in both the workpiece and the coil.

The frequency of the alternating current (AC) used in induction heating systems play crucial roles in determining the heating process and its characteristics. In induction heating, the frequency influences the depth of penetration of the induced current and the heating pattern. High-frequency currents result in shallow penetration depths. This means that the induced current flows mainly on the surface of the material, resulting in surface heating. Low-frequency currents result in deeper penetration depths. The induced current can penetrate deeper into the material, leading to bulk heating [12].

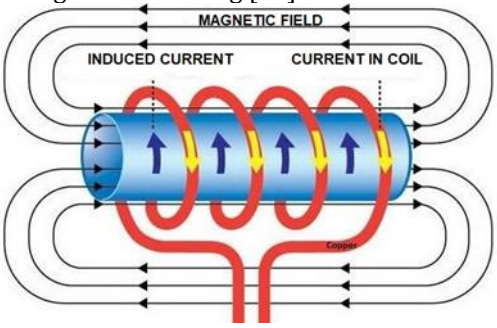

Fig. 1. Different parts of the induction heating system.

In the present work, using the finite element method (FEM) and comsol multiphysics software, we have investigated the effect of different frequencies on the components of induced currents as well as the heat produced in the work piece in three dimensions.

2. Mathematical Formalism

2.1. Governing equation

In order to calculate electromagnetic fields, Maxwell's equations should be solved. Here, we apply following assumptions: a) All materials are linear, isotopic, and non-magnetic. b) There is no net charge. c) Displacement current is not considered. Under these assumptions, Maxwell's equations take forms as follow [2,4,5]:

$$\nabla \cdot \boldsymbol{E} = 0 \quad (1)$$

$$\nabla \cdot \boldsymbol{B} = 0 \quad (2)$$

$$\nabla \times \boldsymbol{E} = -\frac{\partial \boldsymbol{B}}{\partial t} \quad (3)$$

$$\nabla \times \boldsymbol{B} = \mu_0 \boldsymbol{J} \quad (4)$$

Where, E, B, μ, and J are electric field intensity (V/m), magnetic flux density (T), magnetic permeability (H/m), and current density (A/m^2); respectively. By considering equations 1-4, and using $\boldsymbol{B} = \boldsymbol{\nabla} \times \boldsymbol{A}$, $\boldsymbol{A}$ is denoted as magnetic vector potential (Web/m), we can obtain an equation based on vector potential as follows in the whole system:

$$\nabla^2 \boldsymbol{A} + \omega^2 \mu \varepsilon \boldsymbol{A} - i\mu\omega\sigma \boldsymbol{A} = -\mu \boldsymbol{J}_{ext} \quad (5)$$

Here, ω is angular frequency (rad/s), ε is permittivity (F/m), σ is electrical conductivity (S/m), $\mathbf{J}_{\text{ext}}$ is applied current to the coil, and $i(=\sqrt{-1})$ is complex unit. In the latter equation we can ignore the second term on the left side. By employing sinusoidal voltage, the form of vector potential will be:

$$\boldsymbol{A} = (r, z, t) = \boldsymbol{A_0}(r, z)\, exp(i\omega t) \quad (6)$$

$\boldsymbol{A_0}(r, z)$ is denoted as complex amplitude in cylindrical coordinates. By applying $\boldsymbol{A_0} = 0$ in the far away area $(r, z \to \infty)$ and at the axis of symmetry $(r{=}0)$ as boundary conditions and considering self-inductance effect of coil, the total current in the coil is:

$$\boldsymbol{J}_{total}^{coil} = \boldsymbol{J}_{eddy} + \boldsymbol{J}_{ext} \quad (7)$$

Where $\boldsymbol{J_{eddy}} = 0$ is induced current in the workpiece and coil it is obtained from:

$$\boldsymbol{J}_{eddy} = -\sigma_W \frac{\partial \boldsymbol{A}}{\partial t} \quad (8)$$

σ is electrical conductivity of coil or workpiece. In order to calculate produced heat in metallic parts, the following relations are used:

$$Q_{Coil} = \frac{|-i\omega\sigma \boldsymbol{A}_0 + \boldsymbol{J_0}|^2}{2\sigma} \quad (9)$$

$$Q_W = \frac{|-i\omega\sigma \boldsymbol{A}_0|^2}{2\sigma} \quad (10)$$

$\boldsymbol{J}_0$is amplitude of current density of $\boldsymbol{J}_{ext}$ [1,13,14].

2.2. Calculations conditions

Fig.2 presents a schematic of the computed model (in 3-D) as well as the mesh domain. We have utilized a copper coil with an electrical conductivity of $\sigma_{co} = 5.9 \times 10^{+7}(\mathrm{S/m})$ and a stainless steel workpiece with electrical conductivity of $\sigma_w = 4.0 \times 10^{+6}(S/m)$ [2]. In this paper, we have considered several different frequencies: 0.75, 1, 2, 3, and 5 (kHz). The other parameters used in the study are shown in Table.1. It is worth mentioning that one of the significant challenges in simulating induction heating in 3-D is selecting an appropriate mesh size. In our study, after conducting a few trial-and-error iterations based on the geometric properties of the model, we chose a "finer" mesh for the coil and an "extremely fine" mesh for the workpiece.

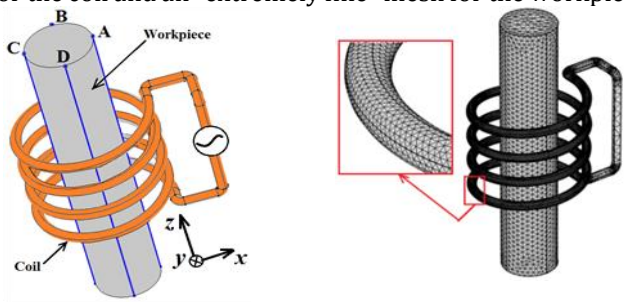

Fig.2 a schematic of computed model (in 3-D) and mesh domain.

Table. 1. Parameters used in the simulation

Description	Symbol	Value
Coil inner radius	R_i	10 [cm]
Coil outer radius	R_o	10.2[cm]
Coil pitch	P_c	5[cm]
Workpiece radius	R_w	5[cm]
Workpiece height	h_w	50[cm]
Voltage	V	200[Volt]
Relative permeability	μ_r	1

3. Results and discussion

We have plotted the profiles of components of induced (eddy) currents in within the workpiece, the amplitude of the induced current profile, as well as the distribution of heat within the workpiece using the finite element method (FEM) and comsol software for different frequencies.

3.1. Eddy Currents in the Workpiece

The eddy current graph is illustrated for three components J_ix, J_iy, and J_iz in the radial direction of the workpiece and the Z=0 plane (P-A). As can be seen, with an increase in frequency, the changes in the J_ix component become more pronounced in the area near the surface of the workpiece (Fig 3.a). Additionally, as one move towards the interior of the workpiece, the patterns of J_ix for frequencies 2-5 kHz differ from those at frequencies 0.75 and 1 kHz. Based on Fig. 3-b, the maximum value of the J_iy component is associated with a frequency of 0.75 kHz, while the minimum value occurs at a frequency 5 kHz.

Indeed, the maximum value of J_iy at a frequency 0.75 kHz is four times that of which at a frequency 5kHz. The flow direction of the J_iz component is opposite to that of the J_iy component, and its values are also lower. When comparing these three components, it becomes evident that while both J_iy and J_iz components exhibit oscillating behavior in the inner area, the J_ix component shows a completely different behavior.

In addition, these profiles reveal that the contribution of J_iy to the total current density is greater than that of the other components. Fig.4 presents the distribution of induced current components in the radial direction and Z=0, but with an alternative axis (shown as A-P). As shown in Fig. 4-a, the behavior of the J_ix component differs from that in Fig. 3-b. In fact, not only does the intensity of this component (J_ix) increase, but its changes are also less pronounced than those in Fig. 3-a. Additionally, although there are slight similarities between J_ix and the J_iy component in Fig. 3-b, their flow directions are opposite. It should be noted that in Fig. 4-b, while there is no significant difference in terms of intensity between this component and J_ix in Fig. 3, they do not follow the same pattern. Upon observing the J_iz component in this figure and comparing it to Fig. 3, we can conclude that its values experience a significant decrease, and their patterns are not the same.

Since each of the eddy current components differs in terms of intensity and pattern, and their forms change at different positions, we calculate the total eddy current in the radial direction (Fig. 5). As can be observed, the maximum value of the induced current occurs at a frequency of 0.75 kHz, which is located on the surface of the workpiece, while the minimum value corresponds to a frequency of 5 kHz. In addition, considering the equation (11), the intensity of eddy current exponentially decreases from the surface towards the center of the workpiece.

$$J_r = J_0\, exp\left(\frac{-(r_0 - r)}{\delta}\right) \tag{11}$$

Here, J_r is current density at a distance r from workpiece surface, r_0 is the workpiece radius, J_0 denotes the intensity of the current density at the workpiece surface and $\delta[m]$ is referred to as the skin depth. Essentially, the skin depth (δ) indicates the penetration depth of electromagnetic waves within the workpiece. To express the skin-depth, we can utilize:

$$\delta = 503\sqrt{\frac{\rho}{\mu_r f}} \tag{12}$$

where μ_r, f and $\rho\,[\Omega.m]$ are relative magnetic permeability, electrical resistivity of the electrically conductive material, and frequency (Hz), respectively [4, 5].

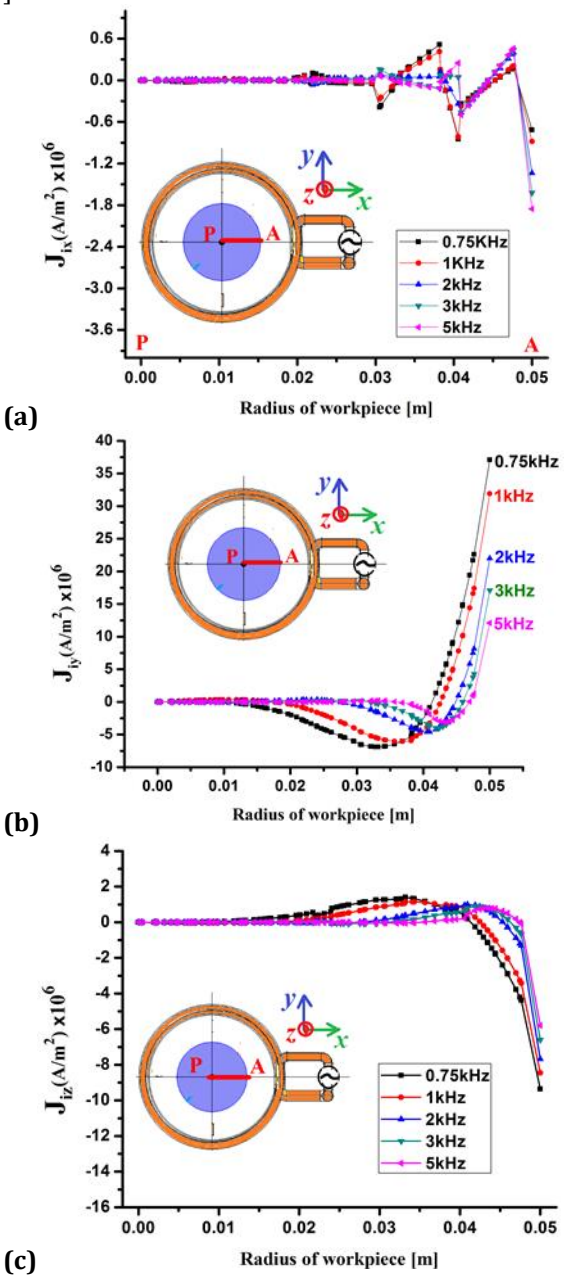

Fig. 3. The profiles of induced current components: (a) J_{ix}, (b) J_{iy}, and (c) J_{iz} in radius direction (P-A, Z=0) for different frequencies.

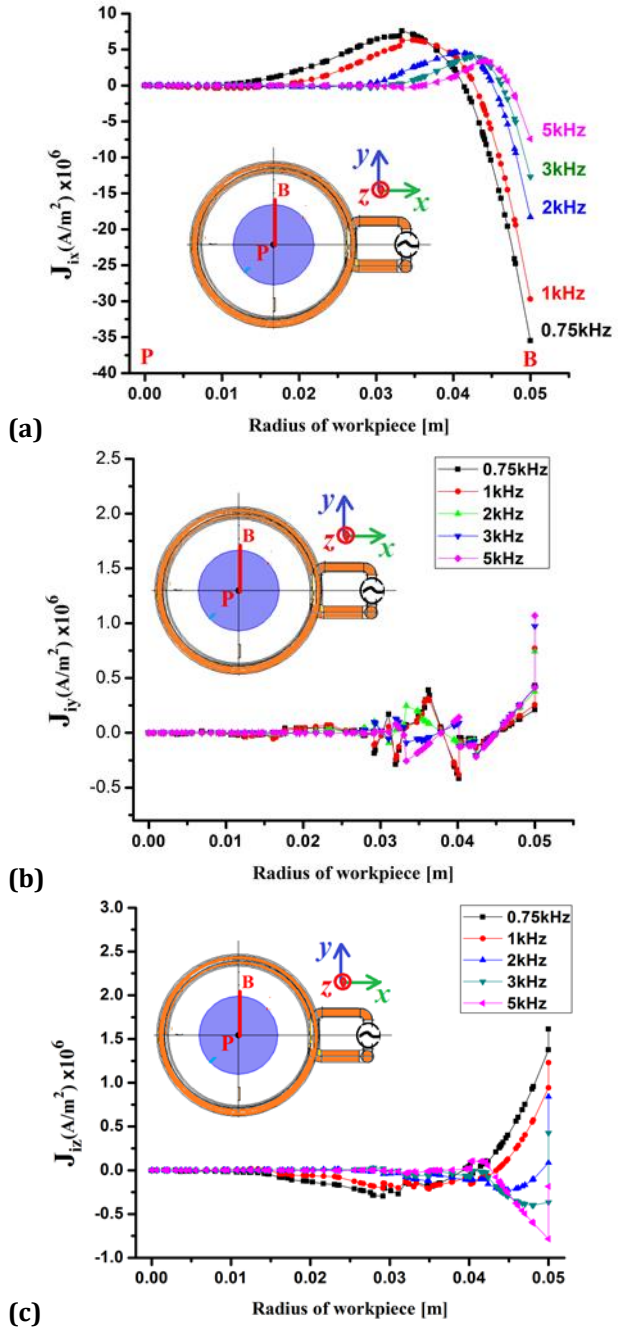

Fig. 4. The profiles of induced current components: (a) J_{ix}, (b) J_{iy}, and (c) J_{iz} in radius direction (P-B, Z=0) for different frequencies.

In Fig.5, the profile of the induced current density in the workpiece for five different frequencies of the voltage applied to the four-ring coil in the radial direction of the workpiece (in the z=0 plane) is drawn using the results obtained from the simulation. The drop of the induced current density from the surface to the center of the workpiece happens exponentially for all frequencies, so that at low frequencies the drop rate is gentler and the penetration depth is greater. Another point that can be seen in this figure is the difference in the current density drop at the frequencies of 0.75 kHz and 1 kHz with the other three frequencies, so that the difference in the depth of penetration between 1 and 2 is greater than other modes. The drop in the induced current density results from damping of the magnetic field inside the conductors. Also, as the frequency increases, the thickness of the penetration depth layer for magnetic fields decreases, so more eddy currents are formed on the surface of the workpiece.

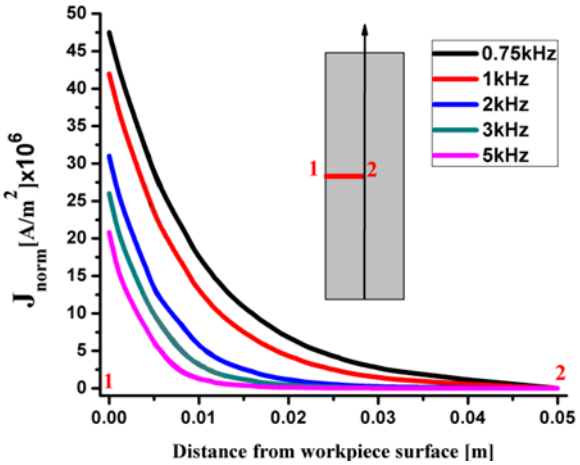

Fig. 5. The induced current total in workpiece radial direction for different frequencies.

3.2. Heat generation in the workpiece

The distribution of generated heat in the workpiece is provided for all considered frequencies, specifically in the radial direction. It can be observed that the trend of heat changes is similar to that of the induced current, following an exponential pattern. However, the values of heat are more than three times that of the eddy current. In the other words, in view of mathematical, while the ratio J_r/J_0 represents the value of eddy current in the interior area of the workpiece corresponding to $1/exp$ of J_0 on its surface, the dissipated power values under this condition will decrease to $1/exp^2$ of its value on the workpiece surface. This is due to the skin effect, which causes approximately 86% of the heat in the workpiece to be concentrated in a surface layer with a thickness δ[4,5]. Additionally, an increase in frequency leads to a decrease in the maximum generated heat, which is concentrated on the surface of the workpiece.

In Figure 6, the heat profile is illustrated in the radial direction, extending from the surface to the center of the workpiece. According to the Joule effect, where heat generation is proportional to the square of the induced current due to the resistance of the metal, the heat generated in the workpiece diminishes significantly in the radial direction. The numerical simulation results of this heat loss are presented in Figure 6. As expected, at higher frequencies, the skin effect becomes more prominent, resulting in shallower penetration depths and concentrated heating near the surface.

The volumetric heat values produced in the coil and workpiece for the desired frequencies are presented in Table 2. Volumetric heat is actually the volume of heat produced in the surface area of the workpiece up to the depth of penetration. As can be seen, the amount of volumetric heat produced is higher at low frequencies. Considering that the depth of penetration decreases with the increase of frequency, therefore, the drastic reduction

of volumetric heat according to Table 2 for the inductor and the work piece is logical. The higher the frequency, the more heat the inductor generates in the work piece.

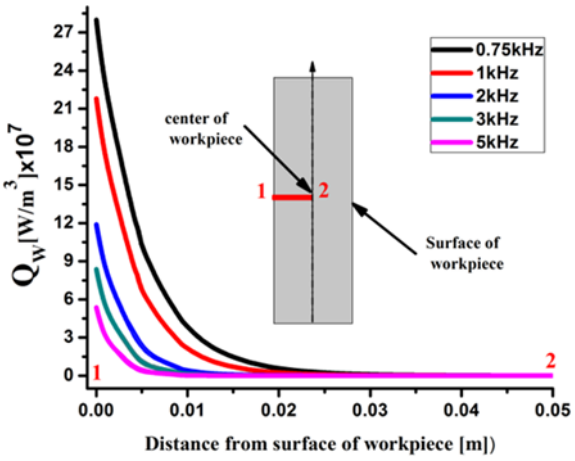

Fig.6. The generated heat distribution in workpiece (radial direction) for different frequencies.

Table 2. Volume integral values of generated heat in the coil and workpiece.

Frequency (kHz)	Coil (kW)	Workpiece (kW)	Efficiency %
0.75	90.69	71.01	43.91
1	58.85	47.96	44.90
2	22.13	18.41	45.41
3	12.48	10.52	45.73
5	6.14	5.21	45.90

4. Conclusion

In the present study, we aimed to investigate the effect of frequency changes on the induction heating process in three-dimensional (real geometry) using the finite element method. To achieve this, we calculated two important quantities: induced current and generated heat in the workpiece. The results obtained from our analysis lead to the following conclusions:

- By examining different directions, such as the radial direction and the plane defined by Z=0, we observed significant changes in the pattern and flow of all induced current components. This highlights the importance of modeling induction heating in a three-dimensional system, as it allows us to gain a more clear understanding of the processes involved in an induction heating system.
- Although the profiles of the total eddy current and heat in the radial direction of the workpiece are similar, the rate of change in heat is twice that of the induced current.
- Increasing the applied frequency results in an improvement in system efficiency.

Acknowledgements

There is nothing to acknowledgement.

Conflicts of Interest

The author declares that there is no conflict of interest regarding the publication of this article.

References

[1] Shokri, A. J. Tavakoli, M. H., Sabouri, A. A., Akhoundikherabad,M. S. 2017. Numerical study of influence of coil step on the induction heating process in three-dimensional, Journal Of Applied Electromagnetic, 27(3), pp 37-44.

[2] Tavakoli, M.H., Karbaschi, H. and Samavat, F., 2011. Influence of workpiece height on the induction heating process. *Mathematical and Computer Modelling*, *54*(1-2), pp.50-58.

[3] Shokri, A.J., Tavakoli, M.H., Sabouri Dodaran, A. and Khezrabad, A., 2019. A numerical study of the effect of the number of turns of coil on the heat produced in the induction heating process in the 3d model. *Iranian Journal of Physics Research*, *18*(3), pp.408-419.

[4] Rudnev, V., Loveless, D. and Cook, R.L., 2017. *Handbook of induction heating*. CRC press.

[5] Lupi, S., Forzan, M. and Aliferov, A., 2015. Induction and direct resistance heating. *Switzerland: Springer*.

[6] Lucía, O., Maussion, P., Dede, E.J. and Burdío, J.M., 2013. Induction heating technology and its applications: past developments, current technology, and future challenges. *IEEE Transactions on industrial electronics*, *61*(5), pp.2509-2520.

[7] Bordelon, D.E., Goldstein, R.C., Nemkov, V.S., Kumar, A., Jackowski, J.K., DeWeese, T.L. and Ivkov, R., 2011. Modified solenoid coil that efficiently produces high amplitude AC magnetic fields with enhanced uniformity for biomedical applications. *IEEE transactions on magnetics*, *48*(1), pp.47-52.

[8] Heidari, H., Tavakoli, M.H., Sobhani, S.O. and Honarmandnia, M., 2018. Influence of magnetic flux concentrator on the induction heating process in crystal growth systems-geometry investigation. *CrystEngComm*, *20*(48), pp.7857-7865.

[9] Khodamoradi, H., Tavakoli, M.H. and Mohammadi, K., 2015. Influence of crucible and coil geometry on the induction heating process in Czochralski crystal growth system. *Journal of Crystal Growth*, *421*, pp.66-74.

[10] Tavakoli, M.H., Mohammadi-Manesh, E. and Ojaghi, A., 2009. Influence of crucible geometry and position on the induction heating process in crystal growth systems. *Journal of crystal growth*, *311*(17), pp.4281-4288.

[11] Tavakoli, M.H. and Mostagir, T.N., 2012. Computational Study of Induction Heating Process in Crystal Growth Systems—The Role of Input Current Shape. *crucible*, *1*, p.0.

[12] Tavakoli, M.H., Karbaschi, H., Samavat, F. and Mohammadi-Manesh, E., 2010. Numerical study of induction heating in melt growth systems—Frequency

selection. *Journal of crystal growth*, *312*(21), pp.3198-3203.

[13] Zhou, X. and Thomas, B.G., 2013. Measuring heat transfer during spray cooling using controlled induction-heating experiments and computational models. *Applied Mathematical Modelling*, *37*(5), pp.3181-3192.

[14] Heidari, H., Tavakoli, M.H., Shokri, A., Mohamad Moradi, B., Mohammad Sharifi, O. and Asaad, M.J.M., 2020. 3D simulation of the coil geometry effect on the induction heating process in Czochralski crystal growth system. *Crystal Research and Technology*, *55*(3), p.1900147.